electron from the [100] valley to one of the four equivalent valleys at [010], [0$\bar{1}$0], [001], and [00$\bar{1}$] (f scattering) has also been predicted and observed by Onton. However, the involved phonon has a higher average energy (47 meV) than the phonon involved in g scattering, and the photoconductivity minimum falls outside of the energy range studied.

V. CONCLUSION

Extrinsic photoconductivity measurements on phosphorus-doped silicon, between 300 and 650 cm^{-1}, at 4 °K, have enabled us to determine the influence of phonons on the photoconductivity spectra. Photoconduction minima are related to a competitive absorption by phonons, either by single phonons activated by the presence of impurities (358, 405, 433, and 478 cm^{-1}), or by impurity resonant modes (433 cm^{-1}), or by double phonons (525 and 609 cm^{-1}). A photoconductivity minimum (574 cm^{-1}) is due to a decrease in the lifetime of the photoionized carriers by an electron intervalley scattering process with emission of an LA phonon at 26.2 meV (210 cm^{-1}).

Thus, photoconductivity turns out to be a very sensitive and very interesting method to study phonons in lightly doped semiconductors, whereas purely optical experiments require heavily doped and compensated (either chemically or by irradiation) samples.

†Work sponsored in part by the Direction des Recherches et Moyens d'Essais of France under Contract No. 732/68.

[1]E. Burstein, J. J. Oberly, and J. W. Davisson, Phys. Rev. 89, 331 (1953).
[2]R. C. Newman, Advan. Phys. 18, 545 (1969).
[3]R. Le Toullec, thesis (University of Paris, 1968) (unpublished).
[4]G. M. Guichar, C. Sebenne, F. Proix, and M. Balkanski, Phys. Rev. B 5, 422 (1972).
[5]M. Lax and E. Burstein, Phys. Rev. 97, 39 (1955).
[6]J. F. Angress, A. R. Goodwin, and S. B. Smith, Proc. Roy. Soc. (London) A308, 111 (1968).
[7]F. A. Johnson, Proc. Phys. Soc. (London) 73, 265 (1959).
[8]M. Balkanski and M. Nusimovici, Phys. Status Solidi 5, 635 (1964).
[9]G. Dolling, in Symposium on Inelastic Scattering of Neutrons in Solids and Liquids, Chalk River, Canada, 1962 (unpublished).
[10]H. J. Stocker, Solid State Commun. 6, 125 (1968).
[11]A. Onton, Phys. Rev. Letters 22, 288 (1969).
[12]B. N. Brockhouse, Phys. Rev. Letters 2, 256 (1959).

PHYSICAL REVIEW B VOLUME 5, NUMBER 8 15 APRIL 1972

Electronic Structure of Amorphous Si from Photoemission and Optical Studies*

D. T. Pierce† and W. E. Spicer
Stanford Electronics Laboratories, Stanford University, Stanford, California 94305
(Received 9 November 1971; revised manuscript received 24 January 1972)

Photoemission from and optical studies of amorphous Si samples, carefully prepared to minimize the influence of defects, are reported. Photoemission yield and energy distribution curves were obtained from 5.5 to 11.7 eV and reflectance data were measured from 0.4 to 11.8 eV. Optical constants were determined by a Kramers-Kronig analysis. No evidence was found to indicate that the wave vector $\vec{k}$ provides a significant quantum number in amorphous Si.

I. INTRODUCTION

Amorphous Si, like amorphous Ge, has been studied widely and is particularly well suited to an investigation of the effects of the loss of long-range order on the electronic structure. Because silicon is an elemental amorphous semiconductor, the complications of compositional disorder and phase separation are avoided. On the other hand, because amorphous Si preserves the short-range order of the crystal (the tetrahedral coordination), the effect of losing long-range order is emphasized when the properties of the amorphous material are compared to the well-known properties of the crystal.

It is becoming clear that care in the material preparation of amorphous Si and Ge is extremely important and will be discussed here because this point may not yet be sufficiently recognized. The Polk-Turnbull[1] model represents a standard of perfection for amorphous Ge and Si. In this model, each atom is fourfold coordinated and no microvoids are present. In the work on Ge, techniques have been developed[2] by which films that closely approach the Polk-Turnbull standard can be produced and characterized.[3,4] In such samples, microvoids are eliminated and densities approaching those of the crystal are obtained.[2] Such samples have sharp optical-absorption edges and relatively large mo-

bilities and lifetimes as judged from photoconductivity studies.[5] Empirically, it has been found that the following conditions[2,6] are necessary to form such films: (i) slow evaporation rates (≈2 to 5 Å/sec); (ii) fairly good vacuum ($p < 5\times10^{-6}$ Torr during evaporation); (iii) large evaporator-to-substrate distance (≈40 cm), which may be the equivalent of having the evaporated material strike the substrate at near-normal incidence; (iv) substrate temperature within 50 or 100 °C of the crystalization temperature.

If a room-temperature substrate rather than a heated substrate is used, sharp optical-absorption edges[2,7] and relatively good mobilities and lifetimes are obtained; however, the optical-absorption edge may be shifted as much as a few tenths of an electron volt to lower energy. It is also clear from several experiments that such films contain an appreciable number of microvoids that have a definite configuration and geometric arrangement.[3,4] We suggest that the shift in the absorption edge is associated with the presence of these systems of microvoids and, furthermore, we recognize that the presence of these systems may create internal strains resulting in the band-edge shift. It is only recently that the relationship between substrate temperature during deposition and the microvoid density has been appreciated completely. Although some photoemission studies have been made as a function of substrate temperature, little difference has been found to date between a sample formed on a room-temperature substrate and on a heated substrate provided that the other three criteria (listed above) are satisfied.

It is necessary to emphasize sample preparation because it is now clear that the properties of amorphous Ge and Si are very dependent on the preparation conditions. If any of the first three criteria are not followed, the sharp optical-absorption edge may be lost. This is well demonstrated by the experiments of Théye[8] who formed samples at deposition rates much larger (200 Å/sec) than those indicated above (2 Å/sec), and found that no sharp absorption edge appeared after deposition; however, when the evaporation rate was reduced to that prescribed above, a sharp absorption edge was obtained. Although much more work is required, these results suggest that a higher evaporation rate leads to a decreased density and probably a different type and pattern of microvoids.

Because the variations in the samples are caused by their method of preparation, it is important that the results of various measurements be judged in terms of the materials preparation. The most significant distinction to be made is between films that exhibit sharp absorption edges and band edges and those that do not exhibit sharp absorption edges and show evidence of very strong tailing of states, as judged from photoemission experiments. Experience indicates that, if the first three preparation criteria are followed, sharp edges will be obtained; whereas, if they are not followed, strong tailing of states into the gap will be evident. It is important that this distinction be made in view of previous theoretical arguments that tailing of states into the gap is a necessary consequence of a lack of long-range order and, in view of Weaire's[9] recent theoretical results, that destruction of long-range order does not necessarily result in a loss of sharp band edges. These results support Weaire's findings and also indicate that the distortion of the covalent bond in reasonably perfect amorphous Ge and Si is not severe enough to destroy the sharp band edges; however, if the amorphous Ge or Si film is formed so that it differs somewhat strongly from the ideal Polk-Turnbull standard, sharp band edges can be destroyed, with large tailing of states into the gap. It should be emphasized that such tailing is an extrinsic effect caused by defects and not an intrinsic effect caused by loss of long-range order.

Although this discussion of sample preparation may seem overly long to the casual reader, it was necessitated by two articles that appeared recently. The first, by Pierce and Spicer,[10] was a partial report on the results that will be presented here; their principal finding was the lack of evidence for tailing of states in amorphous Si. The second article, by Fischer and Erbudak,[11] reported good evidence for tailing of states in their samples of amorphous Si which were prepared with a much closer (≈6 cm) evaporator-to-substrate distance than the 40 cm listed as a criterion necessary to obtain sufficiently perfect samples so that the sharp edges are not destroyed. The difference in the two results appears to be caused by the degree of perfection of the sample studied.

The optical properties of amorphous Si in the region of the absorption edge have been described by Tauc,[12] Brodsky *et al.*,[13] and recently by Donovan Fischer, and Spicer.[5,6] The optical constants have been measured to 7 eV by Beaglehole and Zavetova[14] and to 12 eV by Philipp[15] but not in ultrahigh vacuum. Here, we present the optical constants determined from a Kramer-Kronig analysis of reflectance measurements from 3.2 to 11.8 eV for amorphous Si prepared *in situ* in ultrahigh vacuum. The reflectance was extended to 0.4 eV with the reflectance-transmittance measurements of Donovan.[16]

II. PHOTOEMISSION MEASUREMENTS

The techniques we used in preparing the amorphous Si films were similar to those used to produce amorphous Si and Ge films that exhibited sharp absorption edges.[7,12] The amorphous Si films were electron-gun evaporated from 100-Ω cm n-type and

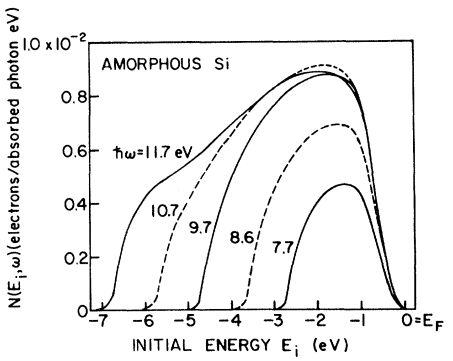

FIG. 1. EDC from amorphous Si with respect to initial-state energy.

1000-Ω cm p-type crystal source materials. The disk-shaped substrates, 0.025 in. thick, were polished, heat-cleaned, Si single crystals [1000 Ω cm (111) n type]. A molybdenum disk was placed between the Cu substrate holder and the substrate because Mo has a lower diffusion into Si. Polycrystalline films formed by annealing the amorphous films and Au films evaporated over the Si served as substrates later in the experiment. The rate of deposition and the film thickness, typically 1000 Å, were monitored with a quartz-crystal microbalance. The base pressure was less than 1×10^{-11} Torr, which rose during evaporation but remained less than 5×10^{-9} Torr, at the typical evaporation rate of 2 Å/sec over a source-to-substrate distance of 48 cm. Evaporations were made onto both room-temperature substrates and those held at 100 °K, using a cooling device previously described.[17]

A conventional retarding-field energy analyzer and a higher-resolution screened-emitter analyzer[18,19] were employed to measure the energy distribution curves (EDC). The EDC is the negative derivative of the current-voltage curve; this derivative is obtained by superimposing a small ac voltage (typically 0.1 V peak to peak) on the retarding voltage and synchronously detecting the resulting in-phase ac component of the photocurrent.[20,21] Higher derivatives can be obtained by detecting higher harmonics of the ac photocurrent.

Energy distribution curves were measured over several photon energies in the $5.5 \leq \hbar\omega \leq 11.7$-eV range. In Fig. 1, typical EDC are plotted with respect to initial-state energy so that the zero of energy corresponds to the Fermi level. The location of the Fermi level is determined if the sample work function is known. The sample work function can be derived from the EDC if the collector work function is known because the difference in sample and collector work functions equals the energy difference between the low-energy cutoff of the EDC and the retarding voltage zero.

It should be emphasized that the EDC obtained from amorphous Si were very reproducible, whether the substrate was single-crystal Si, a polycrystalline film formed by annealing an amorphous film, or a Au film; in addition, no dependence on whether the source material was n type or p type was observed. Similar results were obtained from amorphous films evaporated on substrates at room temperature and at 100 °K, and the EDC were not changed when measured at the two temperatures.

The EDC of amorphous Si (in Fig. 1) are strikingly structureless, especially in comparison to EDC from crystalline Si. A single broad peak is observed at 1.75 eV below the valence-band maximum. At photon energies of 7.7 and 8.6 eV, the photoelectron escape function obscures part of the peak, causing the remainder to exhibit an apparent peak closer to the valence-band maximum. At higher photon energies, the escape function is less effective in the vicinity of the EDC peak.

Third derivatives of the current-voltage curve (second derivatives of the EDC) have been shown to be very useful in detecting subtle structure in EDC.[22,23] If the electronic structure of amorphous Si is simply a "smeared" version of the crystal, some residual peaks might remain. Second derivatives of the EDC were obtained to search for subtle structure in the EDC of amorphous Si. Figure 2 displays EDC from an amorphous and a polycrystalline film at 10.2 eV, along with the second derivatives. None of the typical crystalline structure apparent in the curve from the annealed film is apparent in the curve from the amorphous film.

When EDC from an Si crystal are examined at several photon energies, one finds variations in the position and strength of structure as a result of the conservation of wave vector $\vec{k}$ in the crystal; in the amorphous material, no such variations are found. This is not unexpected because the absence of long-range order in amorphous materials renders the Bloch theorem inapplicable and leaves the crystalline momentum $\hbar\vec{k}$ undefined. We therefore expect the optical transitions to be described to a first approximation by the nondirect transition model in which conservation of energy but not wave vector is significant.[24]

There is no evidence of structure in the EDC produced by structure in the final density of states to which electrons are excited; instead, the single broad peak reflects the valence density of states. We concluded, therefore, that there is no significant structure in the conduction band examined by the EDC (i.e., from 5 to 10.5 eV above the valence-band maximum). The peak at 1.75 eV below the valence-band maximum in Fig. 1 corresponds to a high initial state density at this energy. In this case, the high-energy cutoff corresponds to the valence-band maximum. For amorphous Si, the

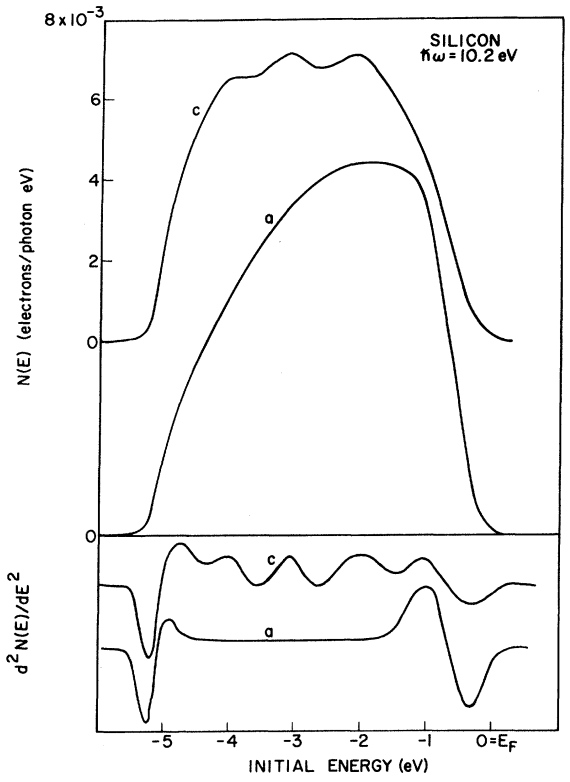

FIG. 2. EDC at $\hbar\omega = 10.2$ eV from an amorphous film (a) and from a polycrystalline film (c) formed by annealing the amorphous film. The second derivative is also shown. None of the typical crystalline structure apparent in the EDC and its second derivative from the annealed film is seen in the EDC and its second derivative from the amorphous film.

Fermi level near the surface (within an electron escape length) was found to be 0.28 ± 0.05 eV above the valence-band maximum.

The optical density of states of amorphous Si can be obtained in terms of the nondirect transition model.[24] In this model, the EDC $N(E, \omega)$ at final energy E and photon energy $\hbar\omega$ is proportional to the product of the density of final states $\rho(E)$ and the density of initial states $\rho(E - \hbar\omega)$. Expressed mathematically,

$$N(E, \omega) = M^2 S(E, \omega)\rho(E)\rho(E - \hbar\omega)/\omega\sigma \ . \qquad (1)$$

Any variation of the dipole matrix elements M, taken as constant, is assumed to be absorbed in the $\rho(E)$ which is referred to, therefore, as the optical density of states. The $N(E, \omega)$ is normalized by the factor $\omega\sigma(\omega)$ which is the optical transition strength

$$\omega\sigma(\omega) = \int_0^{\hbar\omega} M^2 \rho(E)\rho(E - \hbar\omega)\, dE \ . \qquad (2)$$

The threshold or escape function $S(E, \omega)$ determines what fraction of the photoexcited electrons is actually photoemitted into vacuum. This depends on the depth at which the electron is excited [$\sim 1/\alpha(\omega)$], the probability of a collision during travel to the surface, and the minimum momentum normal to the surface required to overcome the surface barrier. The probability of collision is related to the electron attenuation length which, in this case, is expected to be determined by the electron-electron scattering length. The contribution of once-scattered electrons is also included in $S(E, \omega)$. A trial $\rho(E)$ is estimated and used to calculate EDC that are then compared to the experimental EDC over a wide range of photon energies; changes in $\rho(E)$ are made to improve the agreement. In the absence of other information on the scattering length, it is scaled to obtain the best agreement between the experimental yield and the calculated yield

$$Y(\omega) = \int_{E_v}^{\hbar\omega} N(E, \omega)\, dE \ , \qquad (3)$$

where E_v is the experimentally determined vacuum level.

The results of such a calculation of the optical density of states are plotted in Fig. 3. As expected from the EDC in Fig. 1, the valence states display a single broad peak approximately 1.75 eV below the valence-band maximum. Our available photon energy is not high enough to probe into the deep-lying valence states which, by analogy with the crystal valence states,[25,26] are expected to extend to approximately -12 eV. The vertical scale in Fig. 3 is the number of states/eV atom which was set by assuming that the number of states between -5.1 eV and the valence-band maximum is the same as in the crystal.

In Fig. 4, the EDC calculated by using the optical density of states in Fig. 3 and Eq. (1) are compared

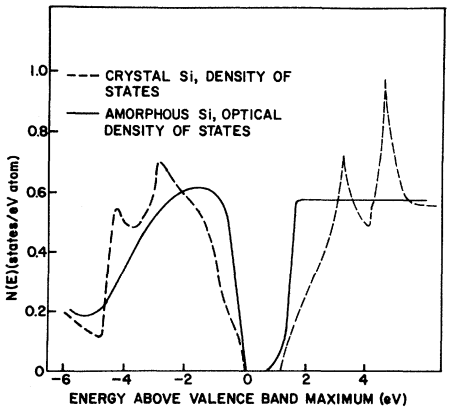

FIG. 3. Optical density of states (solid curve) of amorphous Si, calculated by using the photoemission results of this work compared to the density of states (dashed curve) calculated by Herman *et al.* (Ref. 26) for crystalline Si.

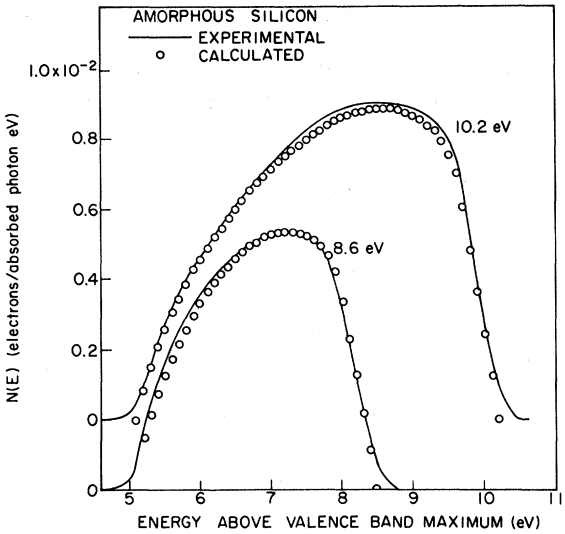

FIG. 4. Experimental EDC (solid curve) and EDC calculated (circles) in terms of the nondirect transition model, using the optical density of states in Fig. 3.

to the experimental curves; agreement both in shape and absolute magnitude is good. A scattering length $L(E)$ of 16 Å at 10 eV was used to determine the escape function $S(E, \omega)$ in Eq. (1).[24]

The conduction-band optical density of states illustrated in Fig. 3 must be taken as a rough model. The EDC do not yield any information concerning the unfilled states up to the vacuum level at 5.1 eV. Some data on this region can be obtained by comparing the imaginary part of the dielectric constant ϵ_2 determined experimentally with that calculated in terms of the nondirect transition model

$$\epsilon_2(\omega) = (C/\omega^2) \int_0^{\hbar\omega} \rho(E)\rho(E - \hbar\omega)\, dE\,, \qquad (4)$$

where C is a constant derived by fitting to experiment at one photon energy. The lower edge of the unfilled states $\rho(E)$ was chosen for best agreement with the leading edge and peak position of the experimental ϵ_2. The maximum value and variation of ϵ_2 suggest that the optical density of states may have a peak located near the conduction-band edge and that the final density of states and/or the optical matrix elements decrease with energy. Because of the oscillator strength sum rule, the matrix elements must decrease at large photon energies.

As noted earlier, no evidence was found for conduction-band structure in the EDC. For simplicity, the conduction-band peak above 2 eV has been drawn as a straight line; this is just a first approximation. The density of states might slant slightly upward or downward; however, any variations from the horizontal line would have to occur in a monotonic fashion.

The density of states calculated by Herman *et al.*[26] for crystalline Si is displayed in Fig. 3 for comparison to our calculated optical density of states for amorphous Si. None of the peaked structure of the crystal density of states is present in the amorphous case. This is not surprising if we consider that the origin of the peaks in the crystal density of states is in the flat-band region (or critical point) near the Brillouin-zone edges; one would expect no such zones in amorphous Si. It is useful to make the distinction discussed by Spicer and Donovan[27] between Bragg and chemical gaps. The peaks of the crystalline density of states are primarily a result of Bragg gaps at Brillouin-zone boundaries which are a consequence of the long-range order. A noteworthy feature of the optical density of states of amorphous Si (displayed in Fig. 3) is the well-defined gap. The short-range order, determined by the covalent bond, appears sufficient to produce a sharp band edge and a well-defined gap.

Theories of amorphous semiconductors have suggested that potential fluctuations caused by disorder give rise to localized states in the energy gap.[28-30] The recent theoretical work of Weaire[9] appropriate to Si has indicated that a tailing of the density of states is not necessarily a result of topological disorder but may be the result of quantitative disorder (variations in bond angles and bond lengths). Theories have not been developed to the point where reliable predictions can be made concerning the number of states in the gap for complex real systems. We have attempted to examine the experimental situation, using photoemission, either to observe the states or to place an upper limit on the number if they are not seen.

Because the EDC reflect the density of valence states in amorphous Si, we can look for a tailing of the density of states into the energy gap by observing the high-energy edge that corresponds to electrons emitted from the top of the filled states. The EDC from the amorphous and polycrystalline films (Fig. 2) have an apparent tail on the high-energy edge resulting from the imperfect resolution found in photoemission measurement systems.[18]

We must distinguish what part of the tail of the EDC is real and what part is a result of imperfect resolution. This can be accomplished by comparing the EDC of an Au film prepared in the same vacuum and measured with the same analyzer geometry and collector surface; the difference between the true edge, known from the Fermi function, and the measured edge will yield a measure of the effect of imperfect resolution. Figure 5 compares an EDC from amorphous Si to an EDC from Au at a photon energy of 6.5 eV. The relative position of the two curves is established by the retarding voltage scale which is the same in each case because the collector work function is the same. The energy scale in Fig.

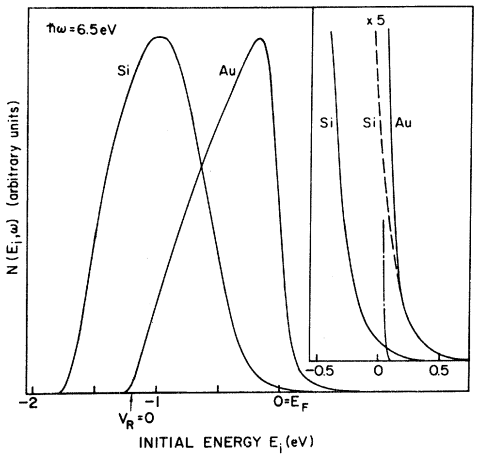

FIG. 5. The effect of instrumental resolution on the high-energy edge is illustrated by comparison between the EDC from Au and amorphous Si at $\hbar\omega = 6.5$ eV. Insert shows the high-energy tails with a 5× magnification of the vertical scale. Dashed curve is the Si tail shifted 0.35 eV higher in energy to overlap the Au tail; the broken curve is the true Fermi function cutoff of the Au. No extra tailing is apparent in the Si, but both Si and Au are resolution broadened compared to the Fermi function cutoff. The point of zero retarding voltage is $V_R = 0$.

5 illustrates the initial state energy of the electrons $E_i = E - \hbar\omega + \varphi$, where E is the measured electron kinetic energy, φ is the work function, and $E_i = 0$ corresponds to the Fermi level E_F. The 1.2-eV measured width of the Au EDC from the low-energy edge to E_F is consistent with $\hbar\omega - \varphi$, where φ is the Au work function independently determined to be 5.3 eV from a Fowler[31] plot of the photoelectric yield. The insert in Fig. 5 displays a 5× vertical magnification of the Si and Au tails and the Fermi tail that corresponds to the undistorted EDC. The measured Au tail extends well beyond the small Fermi tail calculated for the measurement temperature of 130 °K[32]; therefore, it is apparent that the lack of sharpness of the cutoff is the result of instrumental effects. It is the sharpness of the cutoff and not the energy chosen for the valence-band maximum that is important in seeking evidence of tailing.

Normally, the true high-energy cutoff or valence-band maximum is more difficult to determine in a semiconductor than in a metal where the shape is characterized by the Fermi function. Ideally, we would like to derive the exact resolution function which, when convolved with the Fermi function, would obtain the measured Au high-energy edge; we would then deconvolve this resolution function and the measured Si edge to determine the true Si edge. Actually, we had to be satisfied with a rectangular-model resolution function 0.25-eV wide which, when convolved with the linearized Fermi function, produced the slope of the Au EDC edge.[17] When this model resolution function and the Si edge were approximately deconvolved, a valence band edge of 0.28 ± 0.05 eV below E_F was found.

Another way to measure the valence-band maximum to Fermi level energy can be seen in the insert of Fig. 5, where the dashed line is the Si curve that has been shifted 0.35 eV higher in energy to overlap the Au curve. This shift overestimates the valence-band maximum to E_F energy because a piece of the overlapped Au tail stems from a part of the Fermi tail which is above the Fermi energy. A closer look reveals that this 0.35-eV shift is consistent with the 0.28-eV valence-band maximum to E_F energy found above. Because of the overlap of the Si and Au tails, one might suggest that any true undistorted Si tail is also of an exponential form that would be $\exp[-(E - E_F + 0.35\ \text{eV})/0.01\ \text{eV}]$. The density of states from such an exponential tail is $< 10^8$ states/cm^3 eV at E_F and 3×10^{19} states/cm^3 eV at the valence-band edge. In fact, such calculations have little meaning because the noise in the experiment limited the accuracy to which we could compare the Si and Au tails; they might have quite different shapes on a scale less than our experimental detectability.

An upper limit placed on the part of the Si tail that might be caused by a density-of-states tail rather than resolution effects is obtained by estimating the minimum detectable difference between the Au and Si tails, given the noise present in the experiment. To relate the noise level to a number of states, we make use of the optical density of states in Fig. 3 and of the fact that an EDC at 10.2 eV is a good approximation to the optical density of states within 5.1 eV of the valence-band maximum that contains approximately 2.3 electrons. By comparing the quantum yield at photon energies of 10.2 and 6.5 eV, we find that the area of an EDC at 6.5 eV corresponds to 0.15 electrons, and our noise level corresponds to 3×10^{19} states/cm^3 eV which, it should be emphasized, is not an observed density of states but an upper limit found in this experiment. Note that, if the states are concentrated in an 0.1-eV peak in the gap, the number must be less than 3×10^{18} states/cm^3.

In determining this upper bound, the optical matrix elements between localized gap states and the extended conduction states (5 to 6 eV above the conduction-band edge) were assumed to be the same as the matrix elements between extended valence states and the conduction states. A variation of matrix elements would change the upper bound on the states in the gap but would not change the conclusion that no states were observed in our photoemission measurement.

Our conclusion that localized states are not observed differs from the result obtained by Peterson,

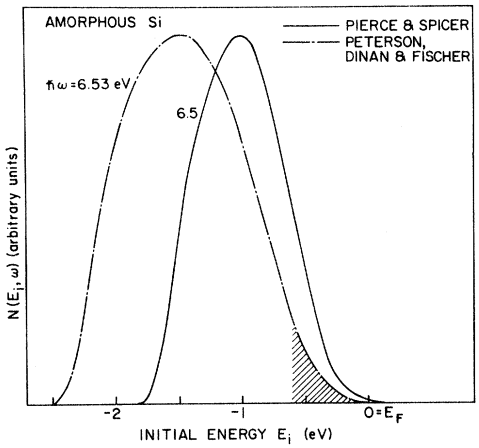

FIG. 6. Comparison between EDC from amorphous Si obtained from our work and results obtained by Peterson, Dinan, and Fischer. Cross-hatched area is attributed to an exponential tailing of the density of states. This area is approximately 10× larger than the area corresponding to our 3×10^{19} states/cm^3 eV upper bound.

Dinan, and Fischer (PDF)[33] and the more recent study of Fischer and Erbudak[11] in which a tailing of localized states is clearly visible up to the Fermi level. Figure 6 compares our EDC at $\hbar\omega = 6.5$ eV to an EDC of PDF at $\hbar\omega = 6.53$ eV which is 0.4 eV wider than ours because of a lower photoelectric threshold. These variances in the photoelectric threshold and in the position of the high-energy edge presumably are caused by the different sample preparation. In the films studied later by Erbudak and Fischer, [11] the high-energy edge of the extended states was 1.1 eV below E_F compared to our 0.28 ± 0.05 eV; also, Fischer and co-workers[11,33,34] found that the photoelectric emission from their freshly deposited amorphous Si films was not reproducible but that reproducible results could be obtained after the films had been annealed for 5 min at 150 °C. In contrast, the photoemission from our films deposited both at 100 °K and at room temperature was reproducible and did not change even when the films were annealed to 250 °C. Fischer *et al.* evaporated their films by passing a current through a Si bar located 1–6 cm from the substrate, while our films were prepared by electron-gun evaporation over a source-to-substrate distance of 48 cm.

PDF suggest that the cross-hatched area between −0.6 eV and the Fermi level is the result of an exponential tail in the density of states; this area is approximately 10 times larger than the area corresponding to our upper limit of 3×10^{19} states/cm^3 eV. Somewhat small tails were observed in later work[11,34] where the evaporation distance was 6 cm instead of the 1 cm used by PDF. The conclusion we draw from this survey of photoemission measurements of amorphous Si is that, although a tailing of the density of states may be caused by a given sample preparation, a tailing larger than our upper limit is not an intrinsic property of amorphous Si; we suggest that is is probably the result of defects in the sample films.

The annealing behavior of amorphous films also produces information concerning the internal defects in the as-deposited film. Adamsky[35] has shown experimentally that, for Ge, the amorphous-to-crystalline transformation temperature is very sensitive to vacuum during evaporation, particularly to oxygen impurities. Nowick[36] has pointed out that the presence of impurities in the amorphous phase, which are insoluble in the crystalline phase, tends to increase the amorphous-crystal transition temperature.

Figure 7[37] plots the effects of annealing as manifested in photoemission EDC from an amorphous film annealed in the same ultrahigh vacuum for 30 min each at measured temperatures of 250, 400, and 550 °C and for 90 min at 625 °C. A separate experiment indicated that, because of radiation losses, the surface of the film could be 10–15 °C, but some over-all change can be seen at 400 °C. Structure characteristic of the crystal appears in the EDC when annealed at 625 °C. The decrease in the slope of the leading edge, seen in Fig. 7, after annealing was more pronounced at lower photon energies.

After the photoemission experiment, further tests were made on the samples. The polycrys-

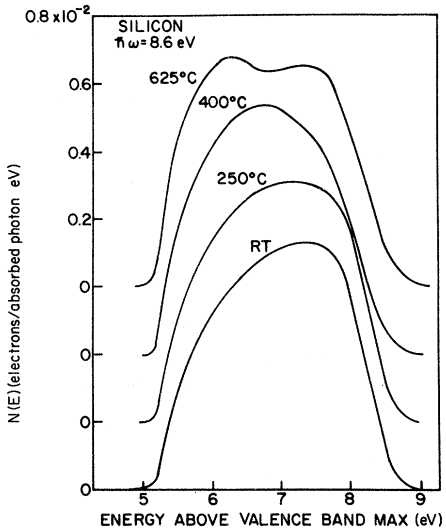

FIG. 7. Photoelectron energy distribution from an as-deposited amorphous Si film (RT) and from the same film annealed at successively higher temperatures until structure characteristic of the crystal appeared.

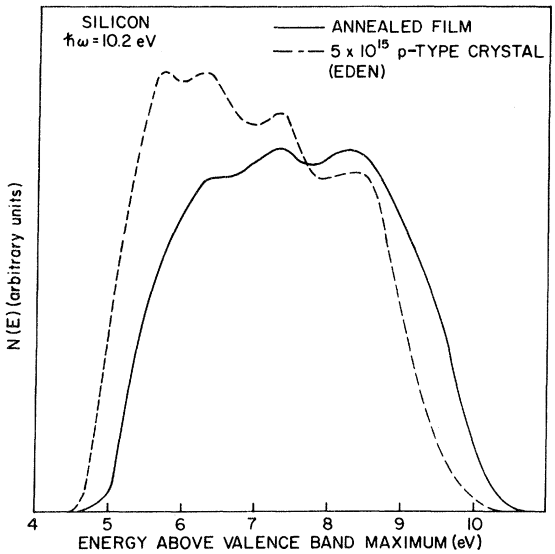

FIG. 8. An EDC from a polycrystalline film (solid curve) formed by annealing the amorphous film to 625 °C compared to an EDC from a cleaved single crystal (dashed curve) measured by Eden.

talline film that had been formed by annealing the amorphous film was checked with x-ray diffraction. This film produced a (220) diffraction peak in addition to a (111) peak which was all that was observed from the single-crystal substrate. Such x-ray diffraction peaks did not appear in the amorphous film. Reflected electron-diffraction patterns showed the characteristic broad halos for the amorphous Si films and sharp rings for the annealed polycrystalline films. The broad halos were also observed in transmission electron diffraction from Si films evaporated onto and floated off KCl substrates.

In Fig. 8, an EDC from a film annealed to 625 °C is compared to an EDC from a 5×10^{15} holes/cm^3 p-type cleaved single crystal measured by Eden.[38] The extra low-energy peak in the single-crystal (dashed) EDC occurs because the photoelectric threshold is lower in the crystal. There is good agreement among the next three peaks in the EDC from the single crystal and from the annealed film; however, the high-energy edge of the curve from the annealed film shows much more strength (almost a shoulder) than the crystal edge determined mostly by the direct transitions possible at that energy. This difference is somewhat puzzling. A likely explanation is that the film annealed at 625 °C is not entirely crystallized. The strength near the leading edge then could result from electrons photoemitted from amorphous regions because EDC of amorphous films show more strength at the edge. This is also a probable explanation for the remarkable similarity (noted in Ref. 10) between the high-energy tails of EDC from amorphous and "polycrystalline" films. At the time of the annealing experiments, it was not possible to go to temperatures higher than 625 °C to see if further annealing changes would appear because of instrumental limitations.

The quantum yield measured from amorphous and annealed films is shown in Fig. 9. At high photon energies, the yield decreases on annealing; at lower energies, it also decreases on annealing but the yield of the polycrystalline film increases. This behavior is quite different from that of Ge, where the yield first increases on annealing and then decreases after annealing at temperatures well above the onset of crystallization.[17]

Recently, Ballantyne[39] has developed a model for photoelectric yield near threshold, which can be applied to amorphous Si. This yield is expected to vary as

$$Y \propto (\hbar\omega - E_T)^3/(\hbar\omega)^2 , \qquad (5)$$

where E_T is the photoelectric threshold. This expression is derived for a rectangular distribution of photoexcited electrons that can be smeared out by phenomenological scattering against phonons, impurities, voids, or surfaces. Our attempts to fit the yield near threshold to a simple power law[40] were unsuccessful, as were the attempts of Peter-

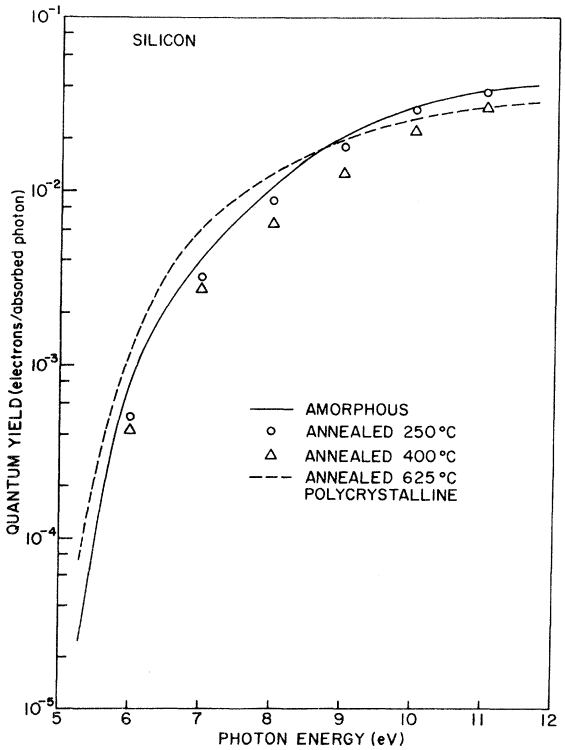

FIG. 9. Quantum yield from an as-deposited amorphous film (solid curve) and from a film annealed to 250 °C (circle), 400 °C (triangle), and 625 °C (dashed curve).

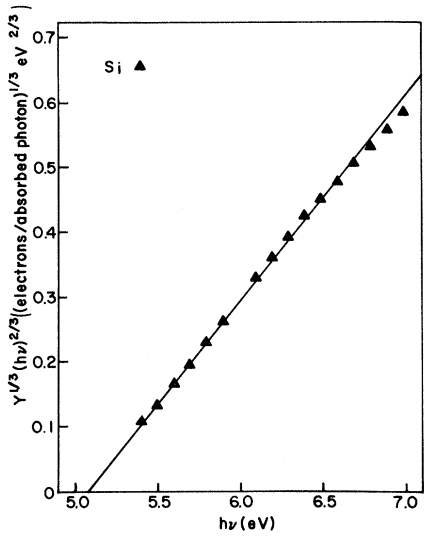

FIG. 10. Yield of amorphous Si near threshold, plotted according to the expression derived by Ballantyne. Threshold determined in this way is 5.08 ± 0.05 eV.

son, Dinan, and Fischer.[33] Using the model of Ballantyne, however, we find it possible to obtain a good straight-line fit to our yield from amorphous Si near threshold, as seen in Fig. 10. The intercept obtains the threshold energy $E_T = 5.08 \pm 0.05$ eV, which is in good agreement with the threshold determined from the width of the EDC. The work function of amorphous Si is 4.8 ± 0.05 eV.

Figure 11 compares an EDC from amorphous Si to an EDC from amorphous Ge[17] at $\hbar\omega = 10.2$ eV. The Ge peak is narrower than the Si peak and is located 1.25 eV below the valence-band maximum, as compared to 1.75 eV for Si. If the peak position is related to the strength of the covalent bond, the position of the Si peak with respect to the Ge peak is in qualitative agreement with the higher "average energy gap" of Si as defined in the dielectric theory

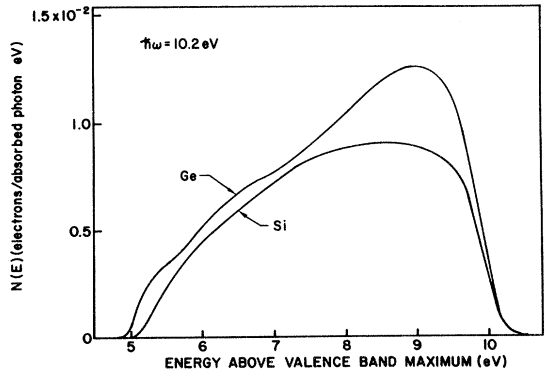

FIG. 11. Photoelectron energy distribution from amorphous Si and amorphous Ge compared at a photon energy of 10.2 eV.

of Phillips.[41] In this theory, the average energy gap E_g is $\hbar\omega_p/(\epsilon_0 - 1)^{1/2}$, where ω_p is the plasma frequency and ϵ_0 is the static dielectric constant. The higher plasma frequency in Si and the lower dielectric constant make E_g larger. The ratio of $E_g(\mathrm{Si})/E_g(\mathrm{Ge})$ is 1.2, compared to the ratio 1.75/1.25 = 1.4. We find this correspondence interesting but, at this point, it is not possible to attach further significance to it.

III. OPTICAL MEASUREMENTS

In Sec. II, the imaginary part of the dielectric constant ϵ_2 was used in determining the shape of the edge of the unfilled optical density of states below 5 eV. We have determined ϵ_2 and other optical functions of amorphous Si from a Kramers-Kronig analysis of normal incidence reflectance data measured over an energy range of $0.4 \leq \hbar\omega \leq 11.8$ eV.

Near-normal incidence reflectance measurements ($\sim 15°$) from 3.2 to 11.8 eV were made on a 600-Å amorphous Si film that was electron-gun evaporated *in situ*. The reflectometer, described by Endriz,[42] is mounted in the same ultrahigh vacuum chamber used for the photoemission measurements. The sodium salicylate phosphor, quartz light pipe, and photomultiplier form the light-detection system of the reflectometer, which directly compares the intensity of the incident light to the intensity of the light reflected from the sample. The reflectance, measured every 0.1 eV, revealed a statistical scatter that indicated a relative measurement accuracy of $\pm 1\%$ which is the absolute accuracy of the reflectometer.[42]

At low photon energies, amorphous Si films rapidly become transparent, and the transmittance as well as the reflectance must be measured. For $\hbar\omega < 3.2$ eV, our reflectance measurements were extended with the precise reflectance and transmittance (RT) measurements of Donovan.[16] His and our reflectance measurements agreed to within 1% in the overlap region of 3.2–5.0 eV; Fig. 12 is the composite reflectance curve. Donovan's re-

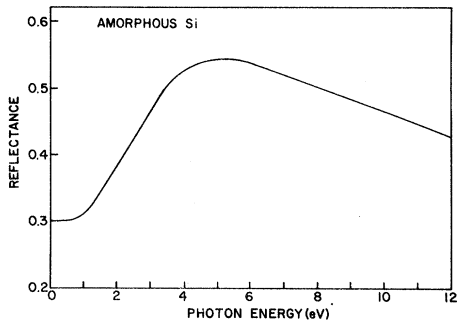

FIG. 12. Reflectance of amorphous Si. The reflectance below 3.2 eV is from the measurements made by Donovan.

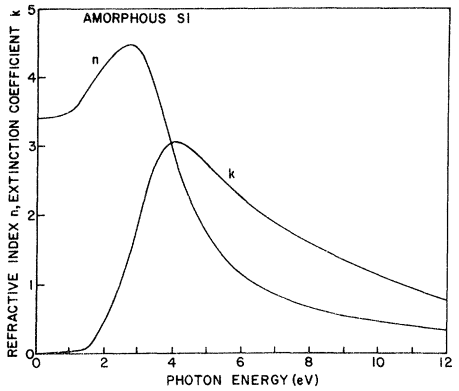

FIG. 13. Real part of the refractive index n and the extinction coefficient k (imaginary part of the refractive index) of amorphous Si, obtained from the Kramers-Kronig analysis.

sults were obtained from amorphous Si films that were electron-gun evaporated in high vacuum and measured in air. The analysis of RT measurements has been described for the case of amorphous Ge.[7]

To determine the optical constants (Fig. 13), the Kramers-Kronig integral[43] was used, which gives the phase θ of the reflected light if the amplitude r is known at all frequencies. The reflectance $R=r^2$ was measured over a finite frequency range, and it was necessary to make extrapolations to zero and infinite frequency. A constant value of R was extrapolated to zero frequency, ignoring the relatively weak contribution from the lattice bands to the optical constants at the higher energies which are of interest to us. Above 12 eV, reflectance was extrapolated by using a power law chosen to give a best fit to the index of refraction $n(\omega)$ and

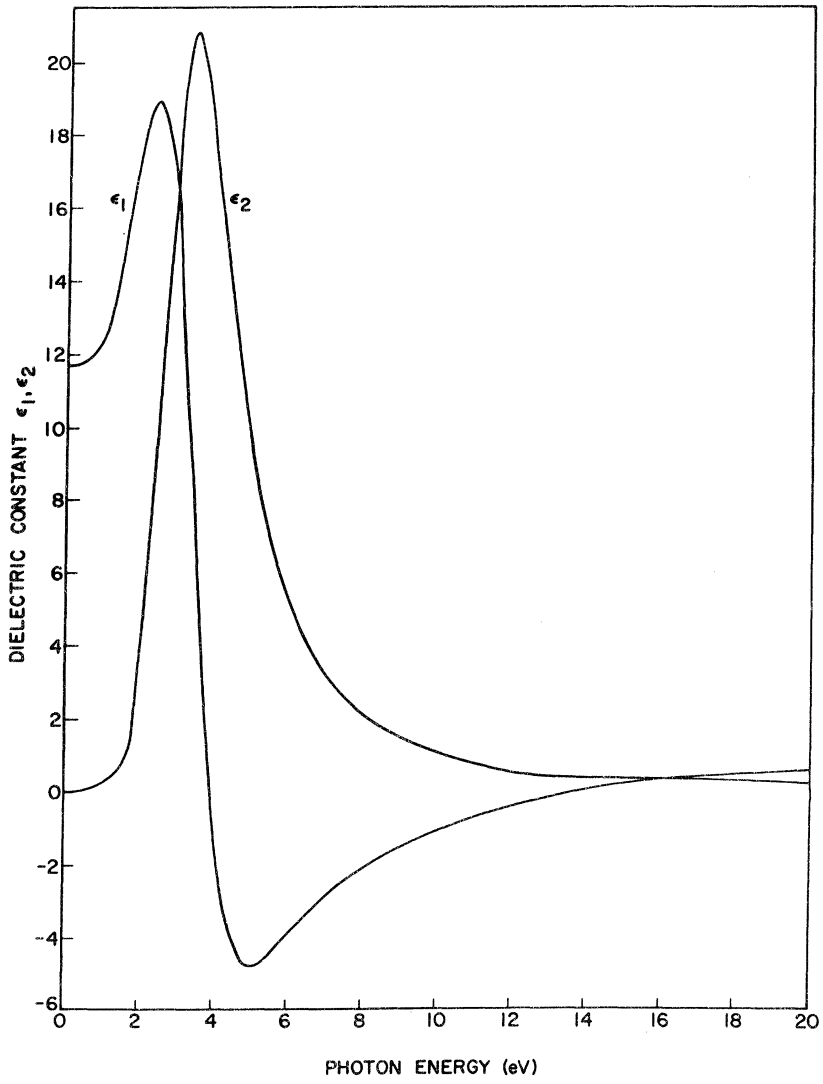

FIG. 14. Real (ϵ_1) and imaginary (ϵ_2) parts of the dielectric constant of amorphous Si.

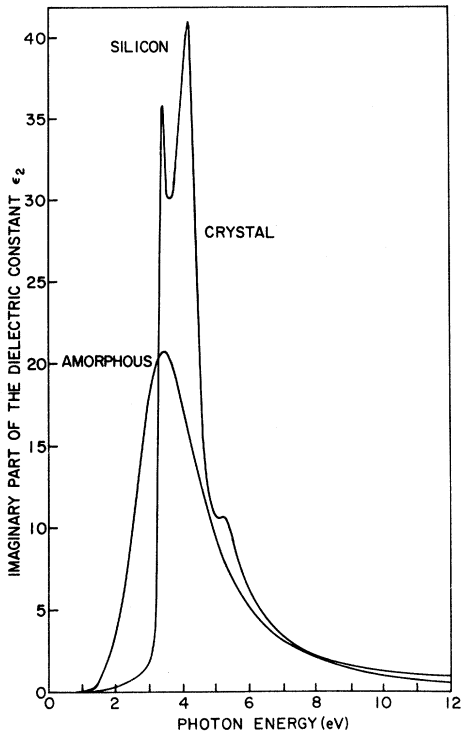

FIG. 15. Imaginary part of the dielectric constant ϵ_2 for amorphous Si compared to ϵ_2 of the crystal measured by Philipp and Ehrenreich.

extinction coefficient $k(\omega)$ determined from the RT measurement of Donovan at 1.0, 1.2, and 4.0 eV.

When $r(\omega)$ and $\theta(\omega)$ are known, $n(\omega)$ and $k(\omega)$ can be determined from

$$n(\omega)=\frac{1-r^2(\omega)}{1+r^2(\omega)-2r(\omega)\cos\theta(\omega)} \tag{6}$$

and

$$k(\omega)=\frac{2r(\omega)\sin\theta(\omega)}{1+r^2(\omega)-2r(\omega)\cos\theta(\omega)}\ . \tag{7}$$

The optical constants of amorphous Si do not show the detailed structure observed in the optical constants of the crystal. The zero-frequency refractive index is 3.4, identical to that in the crystal, and the maximum value of $k(\omega)$ occurs at 4 eV compared to 4.3 eV in the crystal.[44]

Knowing $n(\omega)$ and $k(\omega)$ determines the dielectric constant $\epsilon(\omega)=\epsilon_1(\omega)+i\epsilon_2(\omega)$ because $\epsilon_1=n^2-k^2$ and $\epsilon_2=2nk$. The real and imaginary parts of the dielectric constant are plotted in Fig. 14 out to a photon energy of 20 eV. It should be remembered that portions of the curves above 12 eV are derived from an extrapolation of the reflectance and are less reliable. The maximum in ϵ_2 occurs at 3.5 eV, in good agreement with the value found by Philipp[15] and somewhat higher than the 3.1 eV value in Ref. 14. These variations may be caused by differences in microvoid structure.[4]

The imaginary part of the dielectric constant of crystalline Si indicates detailed structure that can be associated with transitions taking place in specific parts of the Brillouin zone. The smooth ϵ_2 curve of amorphous Si shown in Fig. 14 does not reveal any of this detailed structure. Figure 15 is a closer comparison between ϵ_2 of amorphous Si and ϵ_2 of the crystal.[44] It can be seen that the ϵ_2 of amorphous Si shows more strength than the crystal at lower photon energies and peaks at 3.5 eV; whereas, the center of the strength of the crys-

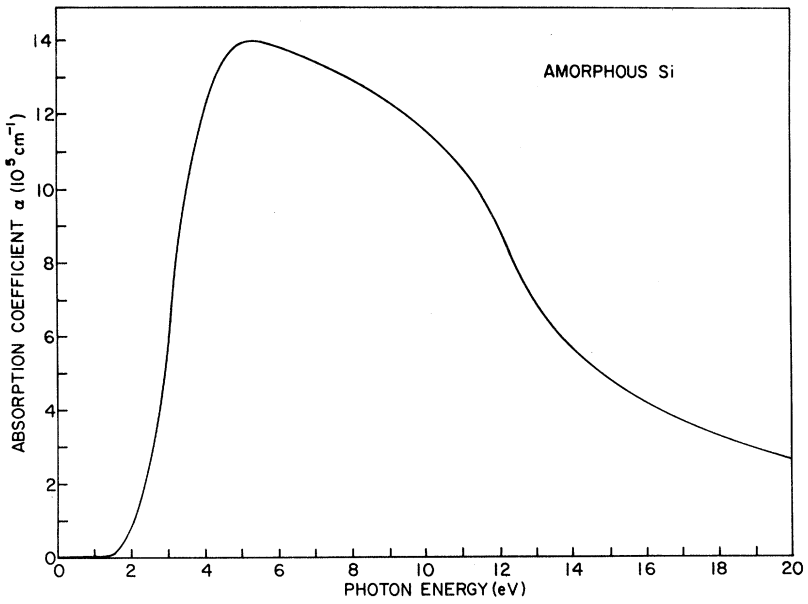

FIG. 16. Optical-absorption coefficient of amorphous Si.

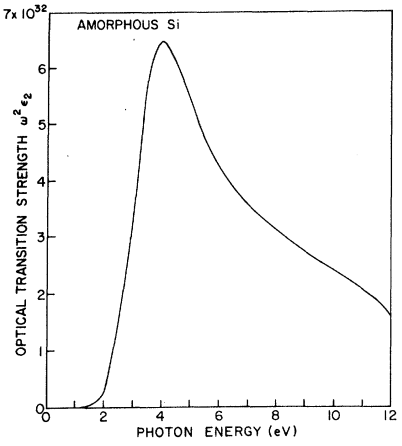

FIG. 17. Optical transition strength $\omega^2\epsilon_2$ for amorphous Si.

talline ϵ_2 curve is at approximately 4 eV. The effect of the lack of long-range order already observed in the EDC from amorphous films also appears clearly in the imaginary part of the dielectric constant. In judging theoretical models of amorphous semiconductors, however, a comparison between theoretical and experimental EDC provides a more sensitive test because the complete set of EDC for a wide energy range contains more information than the ϵ_2 curve.[45]

The optical absorption coefficient $\alpha = 4\pi k/\lambda$ is illustrated in Fig. 16. The need for transmittance in addition to reflectance measurements at low photon energies is clear from the sharp drop in the absorption coefficient. Detailed results in the region of the absorption edge, where the data are best displayed on a log plot, have been reported by Donovan and Fischer[6]; as noted earlier, a sharp absorption edge at approximately 0.6 eV was observed.

The optical transition strength $\omega\sigma(\omega) = \omega^2\epsilon_2(\omega)$ is plotted in Fig. 17. This experimentally determined $\omega\sigma(\omega)$ is used to normalize the EDC calculated on the nondirect transition model [Eq. (1)]. The slight downward turn of the curve near 12 eV is an effect of the extrapolation.

IV. CONCLUSIONS

Our photoemission and optical measurements have presented a consistent picture of the electronic structure of amorphous Si, and the optical density of states has been derived. The loss of long-range order in amorphous Si causes a loss of structure found in the crystal density of states because $\vec{k}$ conservation, in the usual one-particle sense, is not a significant selection rule. The short-range order, however, is apparently sufficient to produce sharp band edges and a well-defined energy gap.

Our photoemission data did not indicate a tailing of the density of states into the gap. Our result differs from others[11] presumably because of variations in sample preparation. We suggest that sample imperfections (principally microvoids) could give rise to an apparent tailing of the density of states but that such states are extrinsic and should be distinguished from a tailing of the density of states produced by only the loss of long-range order.

ACKNOWLEDGMENTS

The authors are grateful to T. M. Donovan and R. C. Eden for sharing their experimental results with us prior to publication. In particular, Donovan's low-energy reflectance and transmittance measurements made possible the Kramers-Kronig analysis of our reflectance measurements to determine the optical functions in the ultraviolet. We have enjoyed helpful discussions with J. M. Ballantyne, T. M. Donovan, J. E. Fischer, T. E. Fischer, M. Erbudak, C. G. Ribbing, G. B. Fisher, and L. F. Wagner. We wish to thank L. Anderson for the electron diffraction measurements and G. Martin for the x-ray diffraction measurements.

---

*Work supported by U. S. Army Research Office (Durham) and the Advanced Research Projects Agency through the Center for Materials Research at Stanford University, Stanford, Calif.

†Present address: ETH, Laboratorium für Festkörperphysik, Hönggerberg, CH-8049 Zürich, Switzerland.

[1](a) D. Turnbull and D. E. Polk, Proceedings of the International Conference on Amorphous and Liquid Semiconductors, Ann Arbor, Michigan, 1971 (unpublished); (b) J. Non-Crystalline Solids (to be published); (c) D. E. Polk, J. Non-Crystalline Solids 5, 365 (1971).

[2]T. M. Donovan, E. J. Ashley, and W. E. Spicer, Phys. Letters 32A, 85 (1970).

[3]T. M. Donovan and K. Heinemann, Phys. Rev. Letters 27, 1794 (1971).

[4]F. J. Galeener, Phys. Rev. Letters 27, 421 (1971); 27, 1716 (1971); R. S. Bauer, F. J. Galeener, and W. E. Spicer, in Ref. 1(a).

[5]J. E. Fischer and T. M. Donovan, Opt. Commun. 3, 116 (1971); in Ref. 1(a).

[6]T. M. Donovan and J. E. Fischer, J. Non-Crystalline Solids (to be published); W. E. Spicer, T. M. Donovan, and J. E. Fischer, *ibid.* (to be published).

[7]T. M. Donovan and W. E. Spicer, Phys. Rev. Letters 22, 1058 (1969); T. M. Donovan, W. E. Spicer, J. M. Bennett, and E. J. Ashley, Phys. Rev. B 2, 397 (1970); W. E. Spicer and T. M. Donovan, J. Non-Crystalline Solids 2, 66 (1970).

[8]M. -L. Théye, Opt. Commun. 2, 329 (1970); Mat. Res. Bull. 6, 103 (1971).

[9]D. Weaire, Phys. Rev. Letters 26, 1541 (1971).

[10]D. T. Pierce and W. E. Spicer, Phys. Rev. Letters 27, 1217 (1971).

[11]T. E. Fischer and M. Erbudak, Phys. Rev. Letters

27, 1220 (1971).
[12]J. Tauc, Mater. Res. Bull. 3, 37 (1968).
[13]M. H. Brodsky, R. S. Title, K. Weiser, and G. D. Pettit, Phys. Rev. B 1, 2632 (1970).
[14]D. Beaglehole and M. Zavetova, J. Non-Crystalline Solids 4, 272 (1970).
[15]H. R. Philipp, J. Phys. Chem. Solids 32, 1935 (1971).
[16]T. M. Donovan (unpublished).
[17]C. G. Ribbing, D. T. Pierce, and W. E. Spicer, Phys. Rev. 4, 4417 (1971).
[18]T. H. DiStefano and D. T. Pierce, Rev. Sci. Instr. 41, 180 (1970).
[19]D. T. Pierce and T. H. DiStefano, Rev. Sci. Instr. 41, 1740 (1970).
[20]W. E. Spicer and C. N. Berglund, Rev. Sci. Instr. 35, 1665 (1964).
[21]R. C. Eden, Rev. Sci. Instr. 41, 252 (1970).
[22]N. V. Smith and M. M. Traum, Phys. Rev. Letters 35, 1017 (1970).
[23]L. D. Laude, B. Fitton, and M. Anderegg, Phys. Rev. Letters 26, 637 (1971).
[24]C. N. Berglund and W. E. Spicer, Phys. Rev. 136, A1030 (1964).
[25]E. O. Kane, Phys. Rev. 146, 558 (1966).
[26]F. Herman, R. L. Kortum, C. D. Kuglin, and J. L. Shay, in *Proceedings of the International Conference on II-VI Semiconducting Compounds, Providence*, 1967 (Benjamin, New York, 1967), pp. 271—289.
[27]W. E. Spicer and T. M. Donovan, Phys. Letters 36A, 459 (1971).
[28]N. F. Mott, Advan. Phys. 16, 1 (1967).
[29]M. H. Cohen, H. Fritzsche, and S. Ovshinsky, Phys. Rev. Letters 22, 1065 (1969).
[30]F. Stern, Phys. Rev. B 3, 2636 (1971).
[31]R. H. Fowler, Phys. Rev. 38, 45 (1931).
[32]The height of the Fermi function in Fig. 5 corresponds to the height of the optical density of states of Au rather than the EDC at 6.5 eV which is diminished by the photoelectron escape function.
[33]C. W. Peterson, J. H. Dinan, and T. E. Fischer, Phys. Rev. Letters 25, 861 (1970).
[34]M. Erbudak and T. E. Fischer, J. Non-Crystalline Solids (to be published).
[35]R. F. Adamsky, J. Appl. Phys. 40, 4301 (1969).
[36]A. S. Nowick, Solid State Phys. 2, 155 (1970).
[37]In Fig. 7, the yield and reflectance of the amorphous film was used to normalize the EDC from films annealed to 250 and 400 °C.
[38]R. C. Eden (unpublished).
[39]J. M. Ballantyne, Phys. Rev. (to be published).
[40]E. O. Kane, Phys. Rev. 127, 131 (1962).
[41]J. C. Phillips, Phys. Rev. Letters 22, 645 (1969).
[42]J. G. Endriz, Ph. D. thesis (Stanford University, 1970) (unpublished).
[43]F. Stern, in *Solid State Physics*, Vol. 15, edited by F. Seitz and D. Turnbull (Academic, New York, 1963), pp. 299—408.
[44]H. R. Philipp and H. Ehrenreich, Phys. Rev. 129, 1550 (1963).
[45]W. E. Spicer and R. C. Eden, in *Proceedings of the Ninth International Conference on Physics of Semiconductors, Moscow*, 1968 (Nauka, Leningrad, U.S.S.R., 1968), p. 65.

PHYSICAL REVIEW B VOLUME 5, NUMBER 8 15 APRIL 1972

Polaron Bound in a Coulomb Potential*

M. H. Engineer and N. Tzoar
The City College of the City University of New York, New York, New York 10031
(Received 12 October 1971)

We have calculated the shift in ground-state energy of an electron bound in a Coulomb potential in a crystal, to second order in the electron-phonon coupling and for arbitrary values of the electron-impurity coupling.

The problem of an electron, in semiconductors, bound in a Coulomb center and weakly interacting with optic phonons, has been of considerable interest.[1-7] The first term in the perturbative expansion of the ground-state energy in terms of the electron-phonon coupling constant is a function of the electron-impurity coupling. We have calculated this term exactly. Our result, for the ground-state energy, is in amazingly good agreement with the energy shift obtained using lowest-order effective-mass theory.[2] In this theory, the energy shift is calculated by replacing the conduction-band effective mass at the bottom of the band by the free-polaron mass at zero momentum. Another approach (Platzman-Sak[1,3]) is to develop the exact expression of second-order perturbation theory in the electron-phonon coupling as a power series in the electron-impurity coupling β. The first term in this series is identical to that obtained using effective-mass theory. The next term ($\sim\beta^4$) has also been calculated. Our exact result is, on the other hand, almost identical to the effective-mass-theory result, for values of the unperturbed ground-state energy E_B, lying between zero and the energy of one optic phonon.

The ground-state energy shift has been calculated, numerically, for arbitrary values of the electron-impurity potential strength. It is compared with the approximate calculations for ΔE. These are (i) a power series in the strength of the impurity